

AD-A143 932

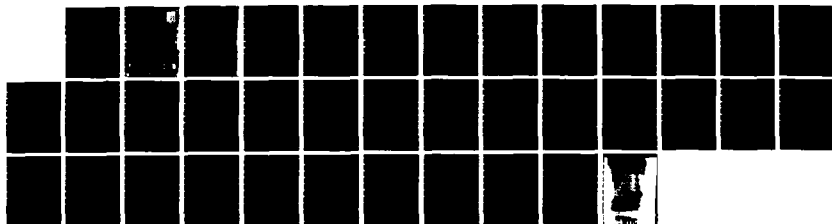
A MODEL OF THE PERFORMANCE CHARACTERISTICS OF
SILICON-GALLIUM INFRARED DE. (U) UNIVERSAL ENERGY
SYSTEMS INC DAYTON OH S MCGUIGAN ET AL. APR 84
AFWAL-TR-84-4035 F33615-82-C-5001

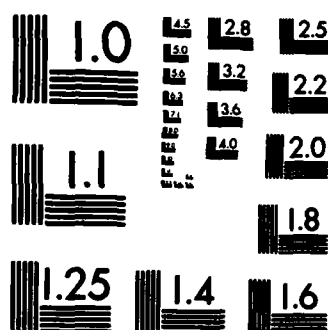
1/1

UNCLASSIFIED

F/G 17/5

NL





MICROCOPY RESOLUTION TEST CHART
NATIONAL BUREAU OF STANDARDS-1963-A

AD-A143 932

AFWAL-TR-84-4035

**A MODEL OF THE PERFORMANCE CHARACTERISTICS
OF SILICON-GALLIUM INFRARED DETECTORS FOR
LOW BACKGROUND APPLICATIONS**



Shaun McGuigan
Universal Energy Systems
4401 Dayton Xenia Road
Dayton, Ohio 45432 U.S.A.

Frank Szmulowicz
University of Dayton
Research Institute
Dayton, Ohio 45469

Patrick M. Hemenger
Materials Laboratory
Air Force Wright Aeronautical Laboratories
Wright-Patterson Air Force Base, Ohio 45433 U.S.A.

April 1984

Interim Report for Period 1 September 1981 - 31 March 1984

Approved for public release; distribution unlimited

MATERIALS LABORATORY
AIR FORCE WRIGHT AERONAUTICAL LABORATORIES
AIR FORCE SYSTEMS COMMAND
WRIGHT-PATTERSON AIR FORCE BASE, OHIO 45433

DTIC
ELECTE

AUG 02 1984

E

02 045


NOTICE

When Government drawings, specifications, or other data are used for any purpose other than in connection with a definitely related Government procurement operation, the United States Government thereby incurs no responsibility nor any obligation whatsoever; and the fact that the government may have formulated, furnished, or in any way supplied the said drawings, specifications, or other data, is not to be regarded by implication or otherwise as in any manner licensing the holder or any other person or corporation, or conveying any rights or permission to manufacture, use, or sell any patented invention that may in any way be related thereto.

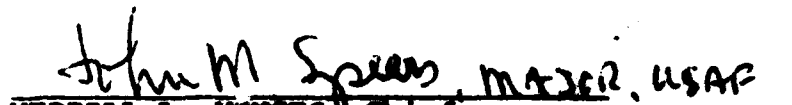
This report has been reviewed by the Office of Public Affairs (ASD/PA) and is releasable to the National Technical Information Service (NTIS). At NTIS, it will be available to the general public, including foreign nationals.

This technical report has been reviewed and is approved for publication.


DAVID W. FISCHER
Project Monitor
Laser & Optical Materials Branch


G. EDWARD KUHL, Chief
Laser & Optical Materials Branch
Electromagnetic Materials Division

FOR THE COMMANDER


MERRILL L. WINGES, Chief
Electromagnetic Materials Division
Materials Laboratory
Air Force Wright Aeronautical Laboratories

"If your address has changed, if you wish to be removed from our mailing list, or if the addressee is no longer employed by your organization please notify AFVAL/NLPO, W-PAFB, OH 45433 to help us maintain a current mailing list".

Copies of this report should not be returned unless return is required by security considerations, contractual obligations, or notice on a specific document.

Unclassified

SECURITY CLASSIFICATION OF THIS PAGE (When Data Entered)

REPORT DOCUMENTATION PAGE		READ INSTRUCTIONS BEFORE COMPLETING FORM
1. REPORT NUMBER AFWAL-TR-84-4035	2. GOVT ACCESSION NO. AD-A143932	3. REPORT'S CATALOG NUMBER
4. TITLE (and Subtitle) A Model of the Performance Characteristics of Silicon-Gallium Infrared Detectors for Low Background Applications		5. TYPE OF REPORT & PERIOD COVERED Interim Report 1 Sept 81 - 31 March 84
7. AUTHOR(s) Shaun McGuigan, Frank Szmulowicz, Patrick M. Hemenger		6. PERFORMING ORG. REPORT NUMBER
9. PERFORMING ORGANIZATION NAME AND ADDRESS Universal Energy Systems, Dayton, OH 45432 Univ. of Dayton Res. Inst., Dayton, OH 45469 Materials Laboratory, WPAFB, OH 45433		8. CONTRACT OR GRANT NUMBER(s) F33615-81-C-5095 F33615-82-C-5001
11. CONTROLLING OFFICE NAME AND ADDRESS Materials Laboratory AFWAL/MLPO Wright-Patterson Air Force Base, Ohio 45433		10. PROGRAM ELEMENT, PROJECT, TASK AREA & WORK UNIT NUMBERS 2306 Q1 06 P.E. 61102F
14. MONITORING AGENCY NAME & ADDRESS (if different from Controlling Office)		12. REPORT DATE April 1984
		13. NUMBER OF PAGES 34
		15. SECURITY CLASS. (of this report) Unclassified
		15a. DECLASSIFICATION/DOWNGRADING SCHEDULE
16. DISTRIBUTION STATEMENT (of this Report) Approved for public release; distribution unlimited		
17. DISTRIBUTION STATEMENT (of the abstract entered in Block 20, if different from Report)		
18. SUPPLEMENTARY NOTES		
19. KEY WORDS (Continue on reverse side if necessary and identify by block number) infrared, IR, silicon, Si, gallium, Ga, boron, B, compensation, detector, responsivity, detectivity, D*, low background		
20. ABSTRACT (Continue on reverse side if necessary and identify by block number) The Si:Ga system is modeled for detection of infrared (IR) radiation in low backgrounds, (10^8 photons/cm ² /sec). The responsivity and detectivity are calculated as functions of residual B, compensation ratio, and temperature. The results demonstrate a large potential for improvement in device performance if starting material with a low residual B is used to manufacture the detectors. These improvements include higher responsivity, higher operating temperature, increased detectivity, greater uniformity in spatial response, and increased radiation hardness.		

DD FORM 1 JAN 73 1473

EDITION OF 1 NOV 65 IS OBSOLETE

Unclassified

SECURITY CLASSIFICATION OF THIS PAGE (When Data Entered)

PREFACE

The work described in this report was supported by Air Force Contract Nos. F33615-81-C-5095 and F33615-82-C-5001 and by in-house Work Unit WUD #48 at the Materials Laboratory, Air Force Wright Aeronautical Laboratories, Wright-Patterson Air Force Base, Ohio. We are indebted to Dr. M. C. Ohmer of the Materials Laboratory and to Dr. Joseph E. Lang and Mr. John A. Detrio of the University of Dayton for many stimulating discussions and continual encouragement. A special note of thanks goes to Ms. Niki Maxwell for a fine and meticulous job in typing the manuscript.

Accession For	
NTIS GRA&I	<input checked="" type="checkbox"/>
DTIC TAB	<input type="checkbox"/>
Unannounced	<input type="checkbox"/>
Justification	
By _____	
Distribution/ _____	
Availability Codes	
Dist	Avail and/or Special
A-1	



TABLE OF CONTENTS

SECTION		PAGE
I	INTRODUCTION	1
II	DETECTOR PARAMETERS	3
	1. Introduction	3
	2. Quantum Efficiency	3
	3. Responsivity	4
	4. Detectivity	5
	5. Detector Backgrounds	5
III	CALCULATION OF D^* AND R	7
IV	RESULTS AND DISCUSSION	12
V	CONCLUSIONS	28
	REFERENCES	30

LIST OF ILLUSTRATIONS

FIGURE		PAGE
1	Schematic diagram of energy level system for Si:Ga photodetector.	8
2	Plot of calculated carrier concentration versus reciprocal temperature for the three cases of (a) undercompensation, (b) equal compensation, and (c) overcompensation of the boron level.	13
3	Plot of $dp/d\phi$ versus temperature for under, equal, and overcompensation of the boron level for $N_B = 1 \times 10^{13} \text{ cm}^{-3}$.	14
4	Plot of calculated ionized impurity concentration versus reciprocal temperature for case (b) in Figure 2.	16
5	Plot of $dp/d\phi$ versus temperature, for under, equal, and overcompensation of the boron level when $N_B = 1 \times 10^{11} \text{ cm}^{-3}$.	17
6	Comparison of $dp/d\phi$ versus temperature for three boron concentrations ($N_B = 10^{11}$, 10^{12} , and 10^{13} cm^{-3}) at equal compensation.	19
7	Plot of $dp/d\phi$ versus compensation ratio ($K = N_D/N_B$) for three boron concentrations, ($N_B = 10^{11}$, 10^{12} , and 10^{13} cm^{-3}).	20
8	Plot of $(dp/pd\phi)^{1/2}$ versus temperature for the three cases (a), (b), and (c) shown in Figure 3.	22
9	Plot of $(dp/pd\phi)^{1/2}$ versus temperature for the three cases (a), (b), and (c) shown in Figure 5.	23
10	Comparison of $(dp/pd\phi)^{1/2}$ versus temperature for the three cases $N_D = N_B = 10^{12} \text{ cm}^{-3}$, $N_D = N_B = 10^{11} \text{ cm}^{-3}$ and $N_D = 5N_B$ ($N_B = 1 \times 10^{11} \text{ cm}^{-3}$).	25
11	Plot of percentage relative error in responsivity versus compensation ratio, K, for an assumed 10% error in compensation for $N_B = 10^{11} \text{ cm}^{-3}$ and $N_B = 10^{13} \text{ cm}^{-3}$.	26

SECTION I

INTRODUCTION

Infrared detectors designed to operate in the low background environments of space are required to survey celestial objects that have effective surface temperatures of 25K to 300K, i.e. the 8-120 μm region of the infrared (IR) spectrum. In this report a model for the assessment of the requirements for these types of IR detectors is explored. The low background environments of space, where the radiant background may be reduced by nine orders of magnitude over endoatmospheric conditions, promotes high detector sensitivities and also produces other unusual detector characteristics which will be discussed. Extrinsic p-type gallium doped silicon, with a peak wavelength of response at 15.0 μm , is of particular interest for low background applications.

To obtain high performance detectors, stringent control of residual impurity concentrations and their compensation must be achieved, while incorporating the maximum concentration of the principal dopant. The residual impurities present are often of the same electrical type as the principal dopant, but with shallower energies. Since, from systems considerations, it is desirable to operate detectors at the highest possible temperature, while maintaining high responsivities and detectivities, the concentration of compensating impurities incorporated into the material must exceed the sum of the concentrations of the shallow impurities, but by as small an amount as possible. This overcompensation is also required because of nonuniformities, of up to 20%, in the concentration of residual acceptor impurities across a wafer. Under these conditions the presence of these shallow impurities can have a strong influence on the temperature dependence of the responsivity which is primarily caused by the changing occupation of these impurities with temperature.

Here we develop a theoretical model of the temperature dependence of the responsivity and detectivity which takes into account the presence of the shallow acceptor boron and the principal dopant

gallium. We explore the behavior of this system under a variety of conditions of under, exact, and overcompensation of the boron level in Si:Ga. Of particular interest is the behavior of such a detector when the concentration of residual boron is reduced from 10^{13}cm^{-3} to 10^{11}cm^{-3} , under various conditions of compensation.

It is found that by reducing the residual shallow impurity, B, considerable leverage is realized in detector performance. For example, the responsivity increases dramatically and just as importantly the responsivity also becomes less sensitive to changes in compensation. In the most practical sense, this means that when material is being processed it can be intentionally overcompensated to improve uniformity, from one detector to the next in an array, while retaining more than adequate responsivity to detect weak signals. Historically, overcompensation has been used as a brute-force method for making devices uniform but often at the expense of responsivity to the point where the mission could only be fulfilled marginally. To illustrate the dramatic performance potential, it is shown that a device with residual B of 10^{11}cm^{-3} has a higher responsivity with 4X overcompensation than does a device with 10^{13}cm^{-3} B at its responsivity peak at 1X compensation. When the 10^{13}cm^{-3} device is overcompensated to 4X, its responsivity is over 100 times lower.

SECTION II

DETECTOR PARAMETERS

1. Introduction

The performance of a photodetector under the conditions of IR photoexcitation is commonly characterized by the responsivity and detectivity of the device. The current responsivity is defined as the ratio of the signal current to the power of the incident radiation and the detectivity as the signal-to-noise ratio per unit incident radiation power.¹ The former parameter reflects the efficiency of conversion of incident radiation into signal current and the latter, the ability to extract the signal from the noise. In addition to these two quantities the detector quantum efficiency is also of importance, since it describes the efficiency of radiation conversion into photoexcited carriers.

2. Quantum Efficiency

The quantum efficiency for a particular impurity species, i , present in a detector with parallel front and rear surfaces, separated by a distance d along the direction of the incident radiation, is given by

$$\eta_i(\lambda) = \frac{(1-R) [1 - \exp(-\sigma_i N_i^O d)]}{1 - R \exp(-\sigma_i N_i^O d)} \quad , \quad (2.1)$$

where R is the reflectivity of silicon, $\sigma_i(\lambda)$ the optical absorption cross section of the impurity species i , and N_i^O the concentration of the impurity, i , that is not ionized. For the case of weak absorption in an optically thin material, i.e. $\sigma_i(\lambda) N_i^O d \ll 1$, this reduces to

$$\eta_i(\lambda) = \sigma_i(\lambda) N_i^O d \quad . \quad (2.2)$$

Thus a figure of merit for extrinsic photodetectors is a high value of $\sigma_i(\lambda) N_i^O d$ for the principal IR active dopant. Therefore, the wavelength dependence of the quantum efficiency reflects the wavelength dependence of the optical absorption cross-section.

3. Responsivity

If the bulk of photodetector is uniformly illuminated, then the density of carriers throughout the bulk should be uniform. For monochromatic light of wavelength λ the incident power is given by

$$P = \phi_s A \frac{hc}{\lambda} \quad , \quad (2.3)$$

where ϕ_s is the incident signal flux and $A=lw$ is the area of the detector exposed to radiation. The signal current is then given by

$$I_s = j_s A' \quad , \quad (2.4)$$

where j_s is the current density and $A'=dw$ is the area normal to the current's direction. For a p-type infrared detector the current density becomes

$$j_s = e\mu p_s E \quad , \quad (2.5)$$

where e is the electronic charge, μ the hole conductivity mobility, p_s the density of signal generated holes, and E the electric field between the electrodes. The density of holes is given by the photo-generation rate $A\eta\phi_s$ multiplied by the hole lifetime τ and divided by the volume of the detector $V=lwd$

$$p_s = A\eta\phi_s\tau/V \quad , \quad (2.6)$$

where η is the quantum efficiency. The responsivity

$$R = I_s/P \quad , \quad (2.7)$$

is related to the materials parameters through equations (2.3), (2.4), (2.5), and (2.6) according to

$$R = \frac{e\lambda}{hc} \eta G \quad , \quad (2.8)$$

where $G=\tau/T_r$ is the gain of the detector and $T_r=l/\mu E$ is the holes' transit time between electrodes. Equation (2.8) is the standard expression for responsivity derived on the assumption of uniform carrier generation throughout the bulk material.

4. Detectivity

The detectivity, D^* , is based on the signal-to-noise ratio of the detector and serves to delineate the limiting performance of the detector. It is defined at a given wavelength by

$$D^* = (I_s/I_N) \sqrt{A\Delta f} / P, \quad (2.9)$$

where I_N is the root-mean-square (r.m.s.) noise current and Δf is the bandwidth of the measuring electronic circuit. The noise current is due to Poisson-statistics governed generation-recombination noise and is given by²

$$I_N = \sqrt{4I_B q G \Delta f}, \quad (2.10)$$

where I_B is the background photon and thermally generated current.³

$$I_B = A' \mu q E (p_{opt} + p_{th}). \quad (2.11)$$

p_{opt} and p_{th} are the optical and thermal carrier concentrations respectively. Combining equations (2.4), (2.5), (2.9), (2.10), and (2.11) yields the following expression for the detectivity

$$D^* = \frac{\eta \lambda}{2hc} \left[\frac{\tau}{(p_{opt} + p_{th})d} \right]^{1/2}. \quad (2.12)$$

The background optically generated carrier concentration can be obtained from equation (2.6) with ϕ_B , the background photon flux, taking the place of ϕ_s ,

$$p_{opt} = \eta \phi_B \tau / d. \quad (2.13)$$

For $p_{opt} \gg p_{th}$, substitution yields the well-known background limited expression, namely

$$D^* = \frac{\lambda}{2hc} \left[\eta / \phi_B \right]^{1/2}. \quad (2.14)$$

5. Detector Backgrounds

The level of background radiation against which an infrared source is viewed has a profound effect in controlling the resistance of extrinsic detector as well as the background noise

engendered by the detector. The background flux density received by the detector depends on its angular view of the background and on its ability to respond to the wavelengths contained in this source. In terms of its relative spectral responsivity, R , referred to its peak wavelength, it may be written as

$$\phi_B = \frac{\Omega}{\pi} \lambda_p \int_0^{\infty} R(\lambda) \frac{Q(\lambda, T)}{T} d\lambda, \quad (2.15)$$

where Ω is the detector's solid angle view of the background, λ_p the wavelength of peak response, and $Q(\lambda, T)$ is the spectral distribution of the background source. For a "black-body" background, $Q(\lambda, T)$ is the Planck's spectral distribution function given by

$$Q(\lambda, T) = \frac{2\pi c}{\lambda^4 [\exp(hc/\lambda kT) - 1]} \quad (2.16)$$

For a normal cone with angle θ

$$\Omega = \pi \sin^2(\theta/2) \quad (2.17)$$

Thus, for an ideal detector, where R is proportional to λ and the wavelength of peak response corresponds to the cut-off wavelength, λ_c , the expression for ϕ_B becomes

$$\phi_B = \sin^2(\lambda/2) \cdot \int_0^{\lambda_c} Q(\lambda, T) d\lambda \quad (2.18)$$

λ_c is given by $\lambda_c = (1.240/\Delta E) \mu\text{m}$ where ΔE is the ionization energy of the infrared acceptor level.

For the low-background environment of space, the optics of conventional telescopes used to collect the infrared signal and to image it on the detector also make a background contribution. However, this may be reduced significantly by using a cooled optics system. The natural background contributions in a space environment include zodiacal dust radiance, atmospheric emission, and charged particle radiation.^{4,5} Thus, low radiant backgrounds encompassing a range from 10^7 - 10^{11} photons $\text{cm}^{-2}\text{s}^{-1}$ may be encountered.

SECTION III CALCULATION OF D* AND R

This section contains a detailed analysis of the three impurity (Ga, B, Donor) silicon systems, illustrating the interaction between detector temperature, flux level, residual boron concentration, and compensating impurity concentration.

The free carrier concentration obtained under steady state conditions is given by the detailed balance of generation and capture processes. The processes we take into account are the optical generation, g_{opt} , the thermal generation, g_{th} , and the capture of carriers, C , from the valence band. The generalized p-type extrinsic silicon detector will consist of a principal detecting acceptor (in this case gallium), shallower acceptor levels and a compensating donor concentration, as shown in Figure 1 for the system under investigation.

The rate equation for the i th acceptor level, when in a steady-state equilibrium with the valence band, can be written as

$$\frac{dN_i^O}{dt} = C_i - g_{th_i} - g_{opt_i} = 0 \quad (3.1)$$

The optical generation rate g_{opt_i} , is given by integration over the incident photon flux, $\phi(\lambda)$,

$$g_{opt_i} = \frac{1}{d} \int_0^\infty \eta_i(\lambda) \phi(\lambda) d\lambda \quad (3.2)$$

where $\phi(\lambda)$ consists of a constant background $\phi_B(\lambda)$ and signal flux $\phi_s(\lambda)$. For weak absorption, which leads to a uniform generation rate across the detector, equation (3.2) reduces to

$$g_{opt} = N_i^O \int_0^\infty \sigma_i(\lambda) \phi(\lambda) d\lambda \quad (3.3)$$

$$= N_i^O \langle \sigma \phi \rangle_i \quad (3.4)$$

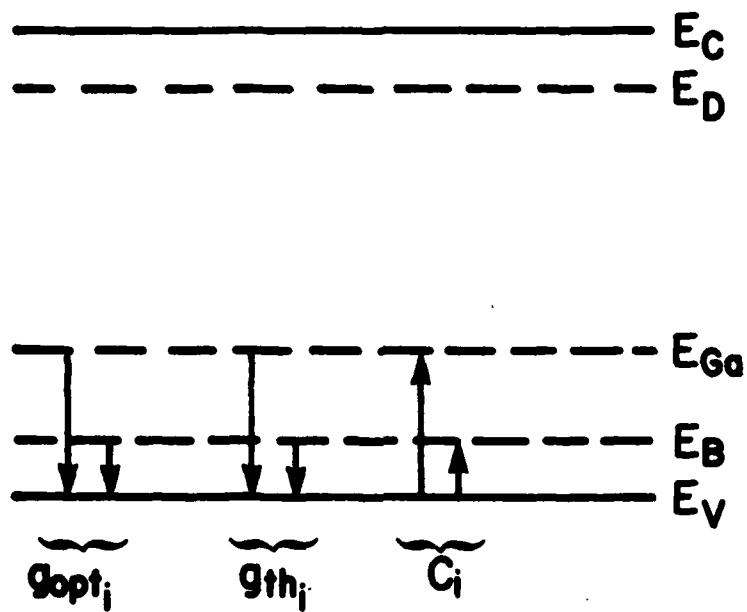


Figure 1. Schematic diagram of energy level system for Si:Ga photodetector.

With the usual expression of Shockley-Read-Hall (SRH) statistics⁶ for thermal generation and capture of free carriers, equation (3.1) may be written as

$$N_i^O \langle \sigma \phi \rangle_i + N_i^O B_i N_V \exp \left[-\frac{E_i}{kT} \right] = p g_i B_i N_i^- \quad (3.5)$$

In equation (3.5), p is the free carrier concentration, N_V is the effective density of states in the valence band^{6,7} and N_i^- , g_i , and B_i are the ionized acceptor concentration, the degeneracy factor and the hole capture coefficient for each impurity species i . With $N_i = N_i^O + N_i^-$ equation (3.5) may be rewritten in the form

$$N_i^- = \frac{N_i}{1 + \frac{g_i p}{N_V e^{-E_i/kT} + \frac{\langle \sigma \phi \rangle_i}{B_i}}} \quad (3.6)$$

Using the charge neutrality condition

$$p + N_D = \sum_i N_i^- \quad (3.7)$$

equation (3.6) can be written as

$$p + N_D = \sum_i \frac{N_i}{1 + \frac{g_i p}{N_V e^{-E_i/kT} + \frac{\langle \sigma \phi \rangle_i}{B_i}}} \quad (3.8)$$

By defining

$$\alpha_{Ga} = \frac{N_V}{g_{Ga}} \exp (-E_{Ga}/kT) + \frac{\langle \sigma \phi \rangle_{Ga}}{g_{Ga} B_{Ga}} \quad (3.9)$$

$$\alpha_B = \frac{N_V}{g_B} \exp (-E_B/kT) + \frac{\langle \sigma \phi \rangle_B}{g_B B_B} \quad (3.10)$$

equation (3.8) can be recast, for a two-level system, as

$$p^3 + p^2(N_D + \alpha_{Ga} + \alpha_B) + p[\alpha_B \alpha_{Ga} - \alpha_{Ga}(N_{Ga} - N_D) - \alpha_B(N_B - N_D)] + \alpha_{Ga} \alpha_B [N_D - N_B - N_{Ga}] = 0 \quad , \quad (3.11)$$

which is most easily solved iteratively using a computer.

On inspecting equations (2.3) through (2.7) in Section II it can be seen that the current responsivity may be expressed as

$$R = \frac{de\mu p_s E}{\phi_s \hbar c} \quad , \quad (3.12)$$

where p_s is the free carrier concentration generated by the signal and may be expressed as

$$p_s = p(\phi_s + \phi_B) - p(\phi_B) \quad . \quad (3.13)$$

Assuming that $\phi_s \ll \phi_B$, p is obtained as

$$p = \left(\frac{\partial p}{\partial \phi} \right)_{\phi_B} \phi_s \quad . \quad (3.14)$$

Substituting equation (3.14) back into (3.12) gives for R

$$R = \left(\frac{e\lambda}{\hbar c} \right) \left(\frac{\mu E d}{l} \right) \left(\frac{\partial p}{\partial \phi} \right)_{\phi_B} \quad . \quad (3.15)$$

Similarly, we may obtain an expression for D^* in terms of $(\partial p / \partial \phi)_{\phi_B}$ by starting from the equation

$$D^* = \frac{\lambda}{\hbar c A \phi_s} \left(\frac{I_s}{I_n} \right) \sqrt{A \Delta f} \quad . \quad (3.16)$$

The detector signal current I_s is given by

$$I_s = A' \mu e E \left(\frac{\partial p}{\partial \phi} \right)_{\phi_B} \phi_s \quad , \quad (3.17)$$

and the noise current, I_N , and background current, I_B , by equations (2.10) and (2.11) respectively. For a compensated detector with a single IR activity impurity, $G = \mu \tau E / l$. However, for the multiple IR active impurity case discussed here, the photoconductive gain is determined as follows.⁸ The photoconductive gain is the

ratio of the number of electrons per second flowing through the detector per photon absorbed in it. Thus,

$$G = \frac{I_s/e}{A\eta\phi_s} = \frac{A' \mu E \left(\frac{\partial p}{\partial \phi} \right)}{A\eta} \quad (3.18)$$

Substituting the above expression for G into the equation for I_N , we obtain

$$D^* = \frac{\lambda}{2hc} \left(\frac{\eta}{p} \frac{\partial p}{\partial \phi} \right)^{1/2} \quad (3.19)$$

Thus, by solving equation (3.11) for p at various temperatures and taking the derivative of equation (3.8) with respect to the photon flux, to give

$$\frac{dp}{d\phi} = \frac{\sum_i \frac{N_i g_i p \sigma_i / B_i}{\left[1 + \frac{g_i p}{N_v e^{-E_i/kT} + \frac{\phi \sigma_i}{B_i}} \right]^2 \left[N_v e^{-E_i/kT} + \frac{\phi \sigma_i}{B_i} \right]^2}}{1 + \sum_i \frac{N_i g_i}{\left[1 + \frac{g_i p}{N_v e^{-E_i/kT} + \frac{\phi \sigma_i}{B_i}} \right]^2 \left[N_v e^{-E_i/kT} + \frac{\phi \sigma_i}{B_i} \right]^2}} \quad (3.20)$$

we may calculate both R and D^* as functions of temperature.

In the derivations of equations (3.15), (3.19), and (3.20) several simplifying assumptions have been made. Firstly, we have assumed that even for the low background environments of space the signal photon flux, ϕ_s , is still much less than the background photon flux, ϕ_B , thus making the detector background limited in its performance. Secondly, in order to differentiate equation (3.8) with respect to the photon flux, we have made the assumption that the majority of the radiant background is absorbed at the peak of the absorption cross-section of the impurity

$$\int_0^\infty \sigma_i(\lambda) \phi(\lambda) d\lambda = \sigma_i(\lambda_p) \phi(\lambda_p) \quad .$$

This is in fact a worst-case scenario and yields values for R and D^* at the peak wavelength of response.

SECTION IV

RESULTS AND DISCUSSION

To investigate the behavior of p and $dp/d\phi$ with doping, temperature and background, we shall consider the specific case shown in Figure 1. Here the gallium is the intentional IR active dopant, present in a concentration of $5 \times 10^{16} \text{ cm}^{-3}$. The residual boron concentration is varied between $1 \times 10^{11} \text{ cm}^{-3}$ and $1 \times 10^{13} \text{ cm}^{-3}$ and the background photon flux level is $1 \times 10^8 \text{ photons cm}^{-2} \text{ s}^{-1}$. The resulting carrier concentration as a function of reciprocal temperature, for the $N_B = 1 \times 10^{13} \text{ cm}^{-3}$ case, is shown in Figure 2 for under, equal, and overcompensation of the boron level. The corresponding variation in $dp/d\phi$ with temperature is shown in Figure 3. It is clearly evident from the four plots in Figure 3 that there are several distinct regimes of behavior in the $dp/d\phi$ versus T plots.

In order to gain a measure of understanding of the $dp/d\phi$ plots presented in Figure 3 one needs to examine the temperature dependence of both the carrier concentration and the ionized impurity concentrations. At liquid helium temperatures, with no background flux present, one assumes that all of the donors are ionized $N_D^+ = N_D$. It therefore follows that for the case of overcompensated boron the ionized gallium concentration will be given by $N_{Ga}^- = N_D - N_B^-$, with $N_B^- = N_B$. Conversely, if the boron level is equally or under compensated then $N_B^- = N_D$ and $N_{Ga}^- = 0$. However, in the presence of background radiation this situation is modified in the following manner. Firstly, holes on both gallium and boron are photoexcited to the valence band from which they may recombine with either ionized boron or gallium. Since the value of σ_i/B_i is approximately the same for both levels, N_i^-/N_i is also approximately the same. This means that $N_B^- \approx N_{Ga}^-$ because $N_{Ga} \gg N_B$. Consequently, the compensation, which originally resided predominantly on boron in the absence of radiation, now shifts to gallium, so that at very low temperatures, $N_{Ga}^- \approx N_D$. We define low temperatures to be below the temperature for significant thermal

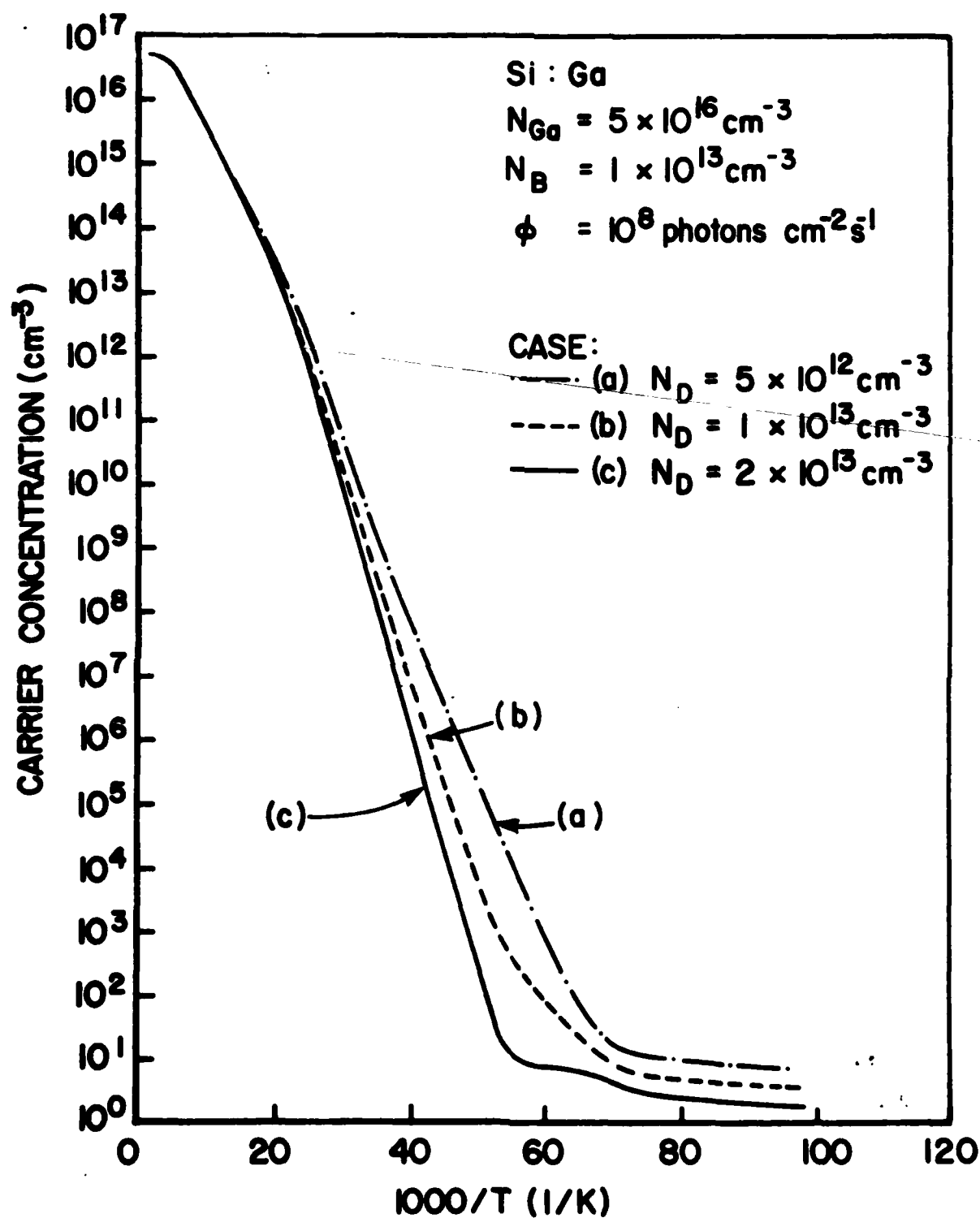


Figure 2. Plot of calculated carrier concentration versus reciprocal temperature for the three cases of (a) under-compensation, (b) equal compensation, and (c) over-compensation of the boron level.

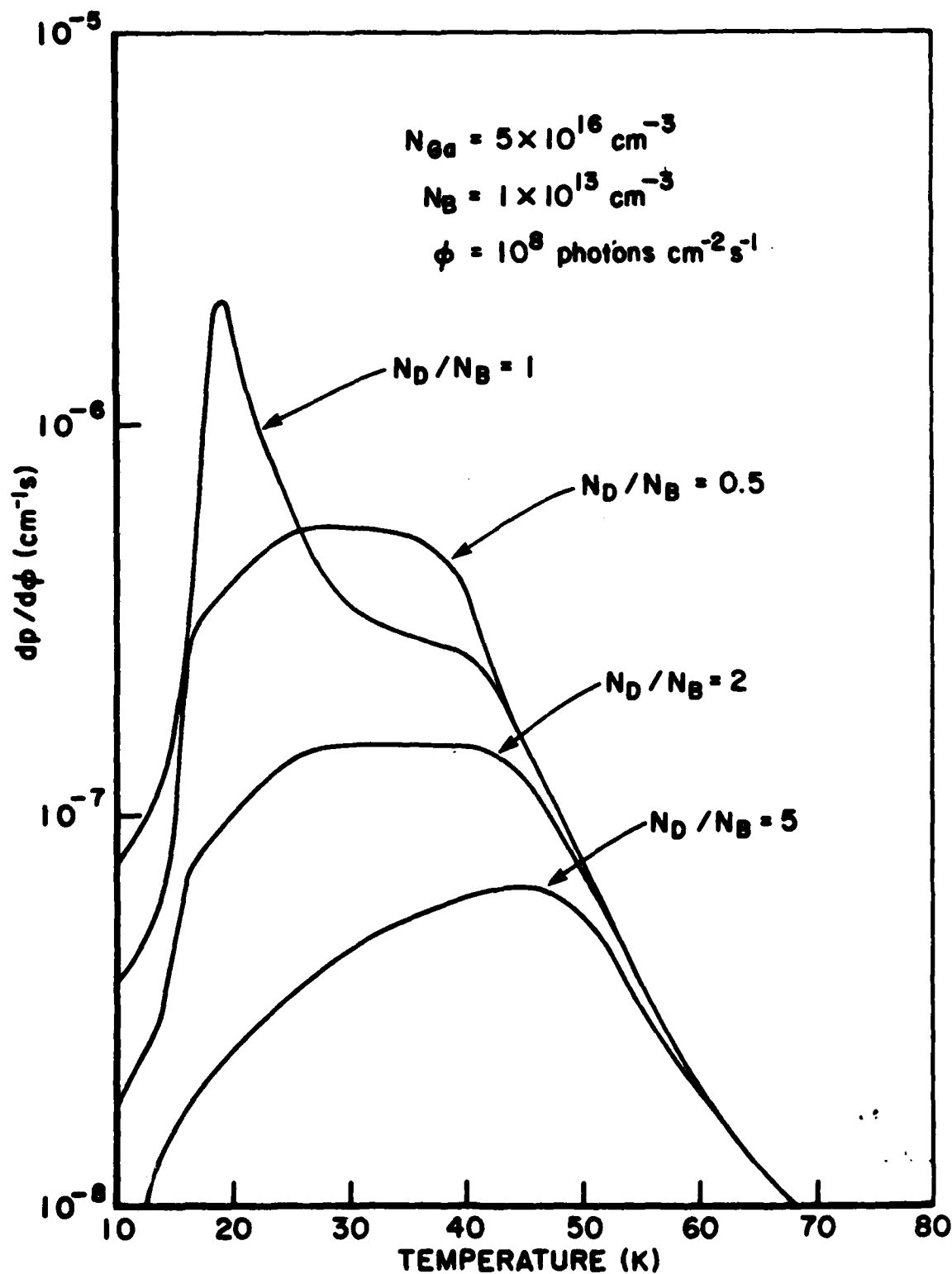


Figure 3. Plot of $dp/d\phi$ versus temperature for under, equal, and overcompensation of the boron level for $N_B = 1 \times 10^{13} \text{ cm}^{-3}$.

depopulation of the boron level, i.e. $T \leq 14K$. This effect can be seen in Figure 4, for the $N_B = N_D = 10^{13} \text{ cm}^{-3}$ case, which shows ionized acceptor concentration as a function of reciprocal temperature.

As the temperature is increased holes are first thermally depopulated from boron to the valence band, since the thermal activation energy for boron, 45 meV, is less than that for gallium, 72 meV. Holes in the valence band are now captured by ionized gallium rather than by ionized boron. This is due to the fact that a hole captured by boron will be rapidly thermally reemitted to the valence band. Therefore, at approximately 19K there is a maximum in the neutral gallium concentration. This leads to higher photoconductive lifetimes since ionized gallium is the principal capture center for holes. This behavior is seen as a dip in the ionized gallium concentration in Figure 4.

With these previous considerations in mind we can interpret the four plots in Figure 3. In each case the very low temperature regime is determined by the compensation residing on the gallium level, $N_G^- \approx N_D$. Therefore, if we keep N_B constant, the photoconductive lifetime will be the longest for material with the lowest donor concentration, as is evident from Figure 3. For $T \leq 14K$ the response is proportional to $1/N_D$. As the process of hole emission from boron and subsequent capture on gallium proceeds for $T > 14K$, the photoconductive lifetime improves and the responsivity increases. Eventually at higher temperatures all of the boron is ionized and no longer acts as an effective capturing center owing to the high probability of thermal reemission of holes from this level to the valence band. Beyond about 30-40K both gallium and boron are strongly thermally depopulated which drastically reduces the photoconductive lifetime. In Figure 3 this corresponds to the sharp fall-off in the responsivity for $T > 40K$.

Figure 5 shows the response for detectors with $N_B = 1 \times 10^{11} \text{ cm}^{-3}$ and same compensation ratios as in Figure 3. Qualitatively the same behavior is seen here as in Figure 3 except that the response in Figure 5 is higher owing to the two orders of magnitude

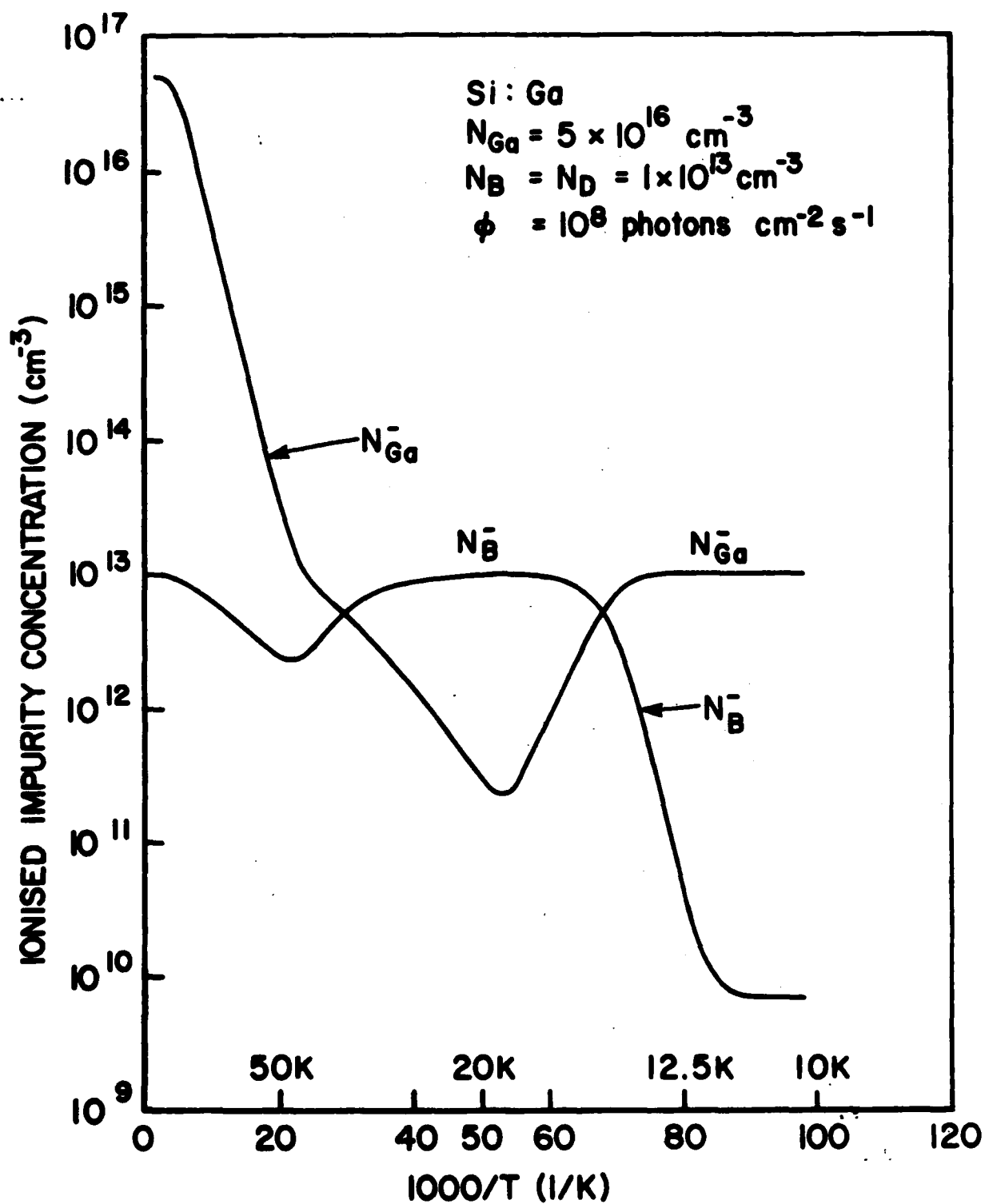


Figure 4. Plot of calculated ionized impurity concentration versus reciprocal temperature for case (b) in Figure 2.

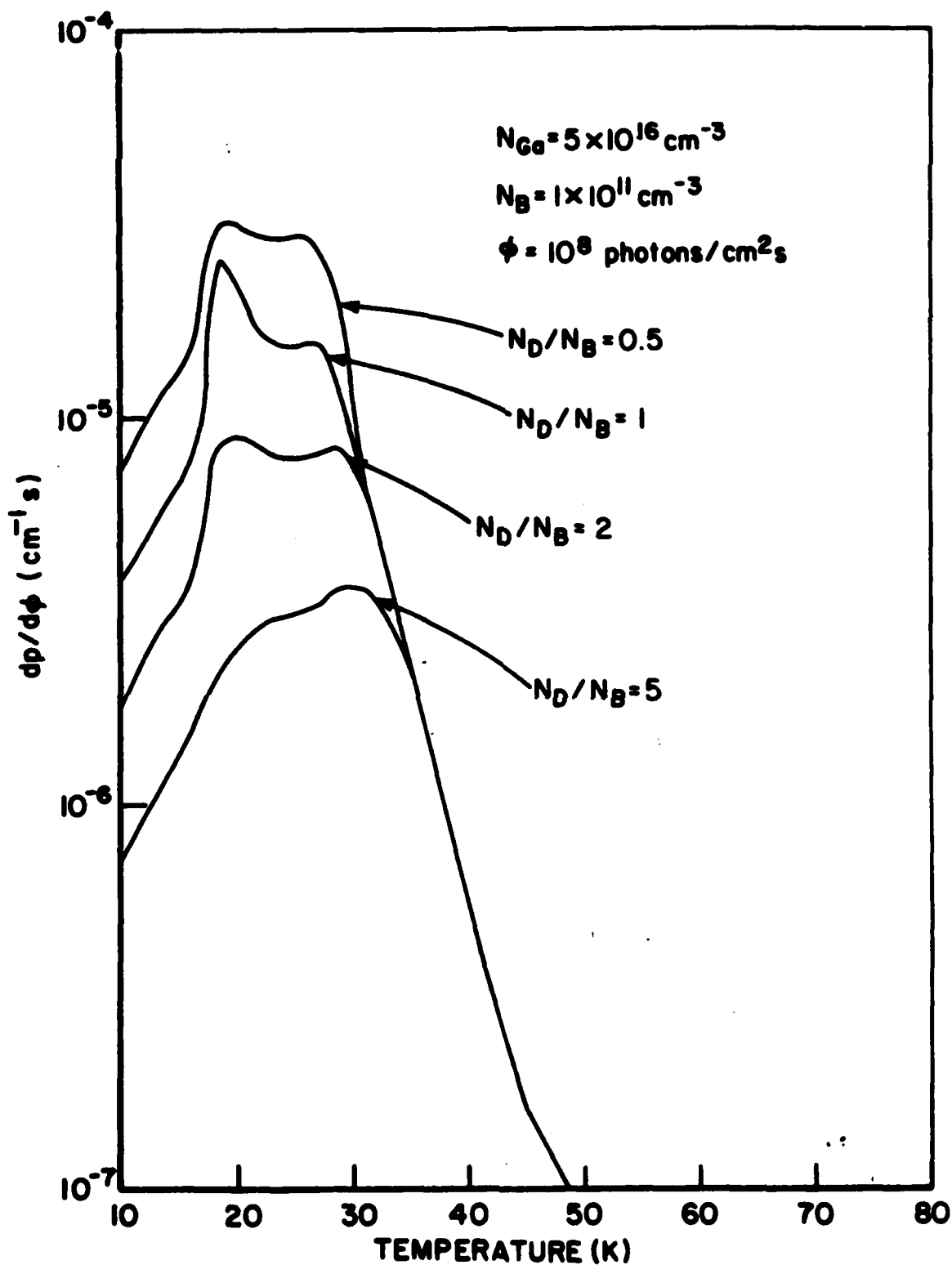


Figure 5. Plot of $dp/d\phi$ versus temperature for under, equal, and overcompensation of the boron level when $N_B = 1 \times 10^{11} \text{ cm}^{-3}$.

reduction in the density of donors. Therefore, the compensation of the gallium level is lower with concomitant beneficial increase in photoconductive lifetime. With the reduction in boron and donor density one also sees that the effects of thermal depopulation of gallium levels produces a rolloff in responsivity at lower temperatures $T > 30\text{K}$ in Figure 5 than in Figure 3 $T > 40\text{K}$. The cause of this effect is clearly shown in Figure 4 which gives the ionized impurity cases for the 10^{13} case at equal compensation. In Figures 3 and 5 the onset of significant rolloff in responsivity occurs when the number of thermally emitted holes exceeds the number of compensating electrons. Therefore, the temperature at which the rolloff effect manifests itself is higher for the higher boron and donor concentration case, but the magnitude of the response is lower.

Figure 6 collects the responsivity curves for three boron concentrations at equal compensation. Clearly, the best response is seen at 19K for the lowest boron doped sample. In going from $N_B = 10^{13}$ to 10^{11}cm^{-3} the response is seen to increase by the factor of 16. Given the simultaneous increase in mobility with less residual boron the actual advantage could be as high as 1600. This assumes the mobility to be limited by the ionized impurity scattering which is proportional to $1/EN_i^-$.

Figure 7 shows peak responsivity for three boron concentrations as a function of compensation ratio. The most important feature of these graphs is the overall increase in responsivity with decreasing boron content. This can be understood as simply being due to an increase in carrier lifetime as a result of the lower donor concentration in the lower boron concentration material. The second notable feature of these plots is the gradual broadening of the responsivity peak at equal compensation. The sharpness of the peak is related to the extent of transfer of compensation from gallium to boron. For the case of high boron concentration, in Figure 4, we see that holes from gallium, which are excited to the valence band, recombine at ionized boron while boron itself is also emitting holes thermally to the valence band. These constitute two competing processes of filling and emptying the boron level. For the lowest boron concentration samples the

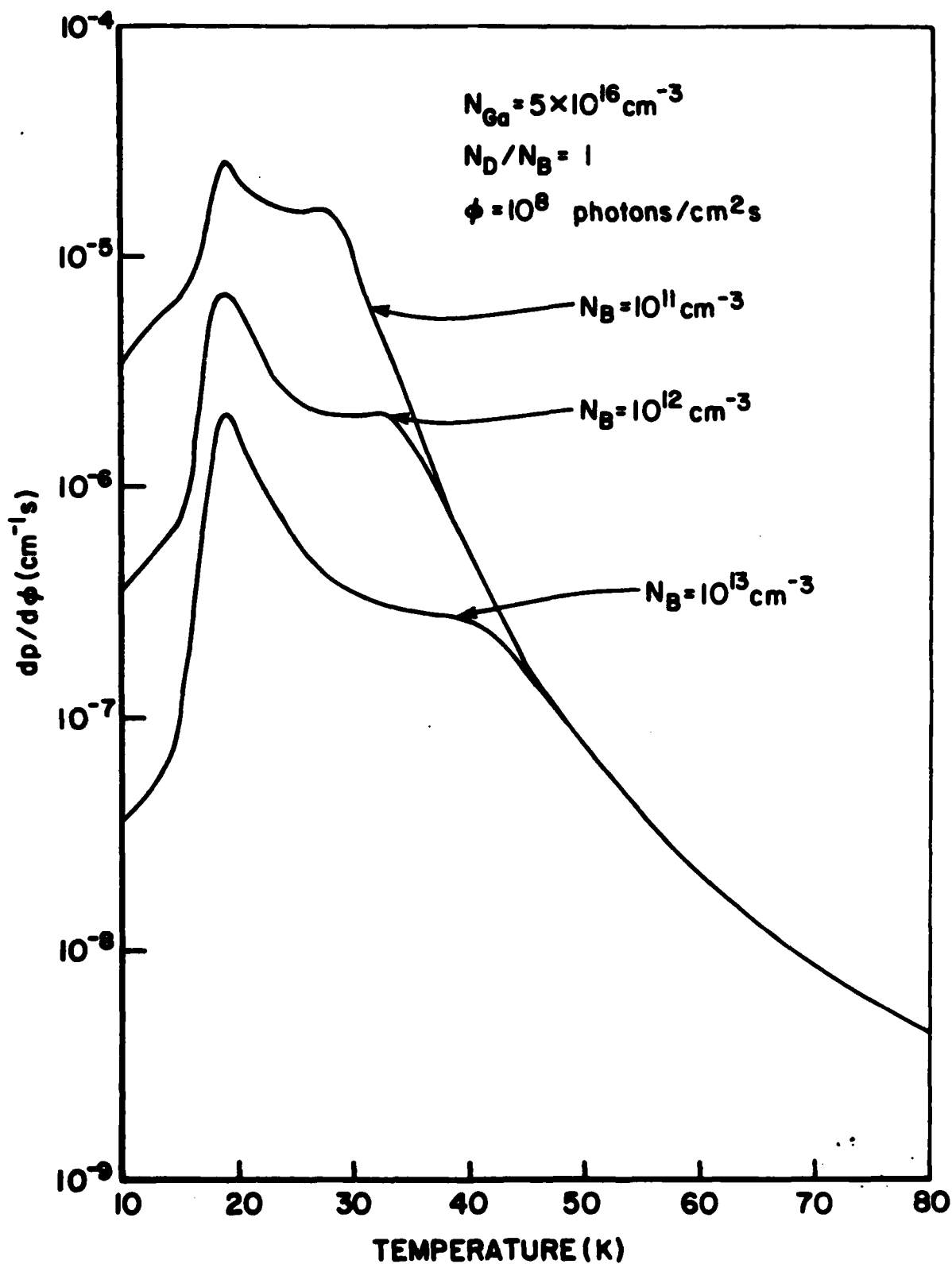


Figure 6. Comparison of $dp/d\phi$ versus temperature for three boron concentrations ($N_B = 10^{11}$, 10^{12} , and 10^{13} cm^{-3}) at equal compensation.

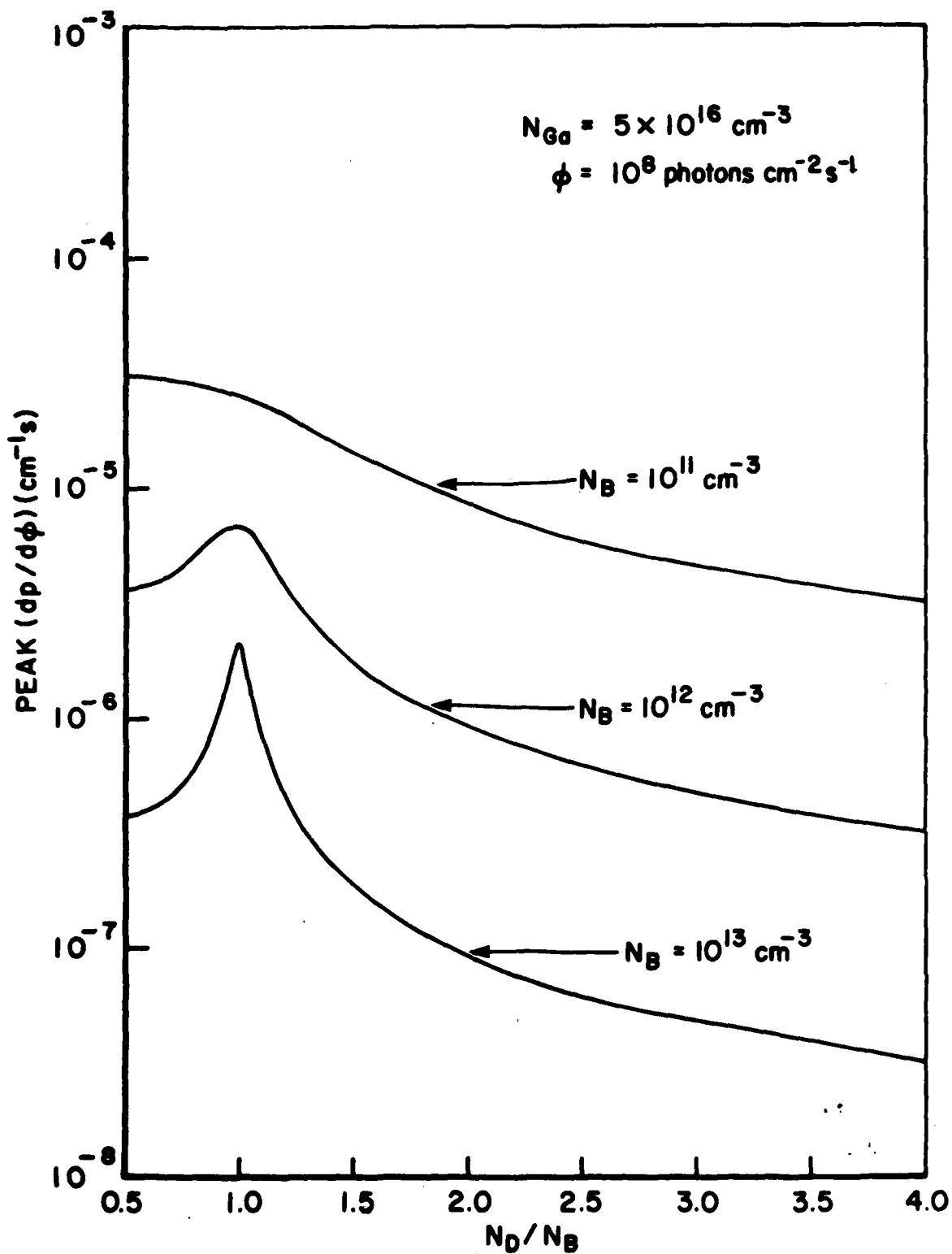


Figure 7. Plot of $dp/d\phi$ versus compensation ratio ($K=N_D/N_B$) for three boron concentrations, ($N_B=10^{11}$, 10^{12} , and 10^{13} cm^{-3}).

rate of population is greater than the rate of depopulation, so that the ionized boron concentration never quite equals the donor concentration. This is primarily due to the fact that the ratio of boron to gallium is low for low boron samples. On the other hand for high boron samples the ratio of boron to gallium is higher, causing the ratio of holes emitted to the valence band by boron to those of gallium to be higher. Thus boron is more effective in shedding its holes in the latter case which has the effect of shifting the compensation from gallium to boron.'

For high boron samples, the exactly compensated case is unique in that the transfer of compensation from gallium to boron is complete. This in turn produces a distinct peak in $dp/d\phi$ vs. $K=N_D/N_B$ plot at $K=1$. In the low boron case since the transfer of compensation is never complete, equal compensation is not distinguished from $K \neq 1$ cases as much, so one does not obtain a distinct peak at $K=1$. The boron concentration at which this latter effect occurs is influenced by the ratio of σ_i/B_i for gallium.

Figure 8 shows the calculated detectivities for $N_B=10^{13}$ and Figure 9 for $N_B=10^{11}$ with varying compensation ratios. In every case D^* is relatively flat until a characteristic temperature where the thermal noise from a rapidly depopulated level produces a sharp rolloff in the detectivity vs. temperature curve. For undercompensated samples the rolloff occurs at lower temperatures since uncompensated boron is the source of the thermally generated holes. For overcompensation one must wait till higher temperatures, where gallium is thermally depopulated, for the rolloff to occur. The flat portion of the curves results from signal increasing at the same rate as the noise. As explained with reference to Figures 1, 2, and 3 the signal increases with increasing temperature due to the increase of photoconductive lifetime for $T < 20K$. But as the photoconductive lifetime increases so does the concentration of thermally and optically produced holes. These holes give rise to the generation-recombination noise. Therefore, as signal increases the noise increases at the same rate and the detectivity is constant.

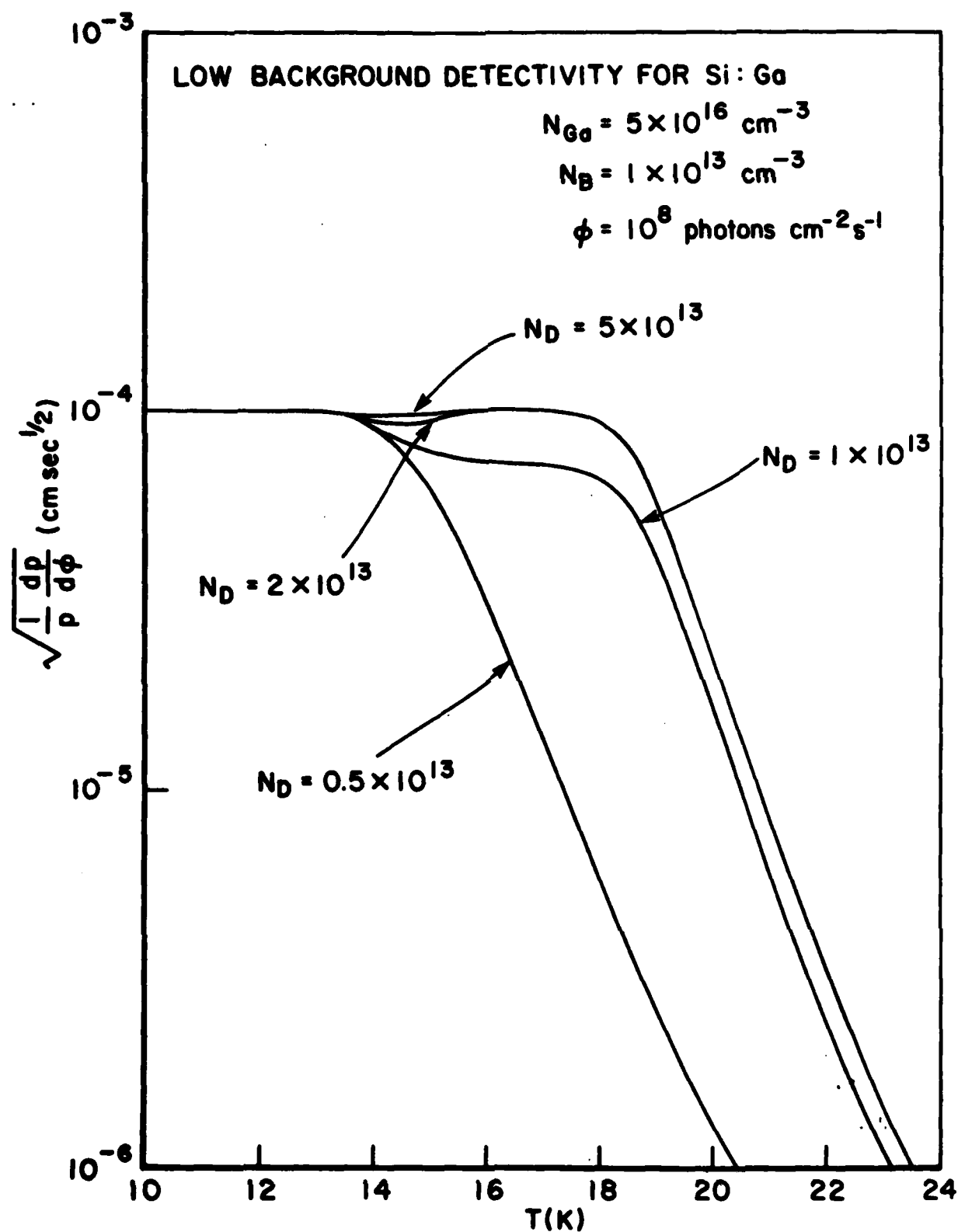


Figure 8. Plot of $(dp/pd\phi)^{1/2}$ versus temperature for the three cases (a), (b), and (c) shown in Figure 3.

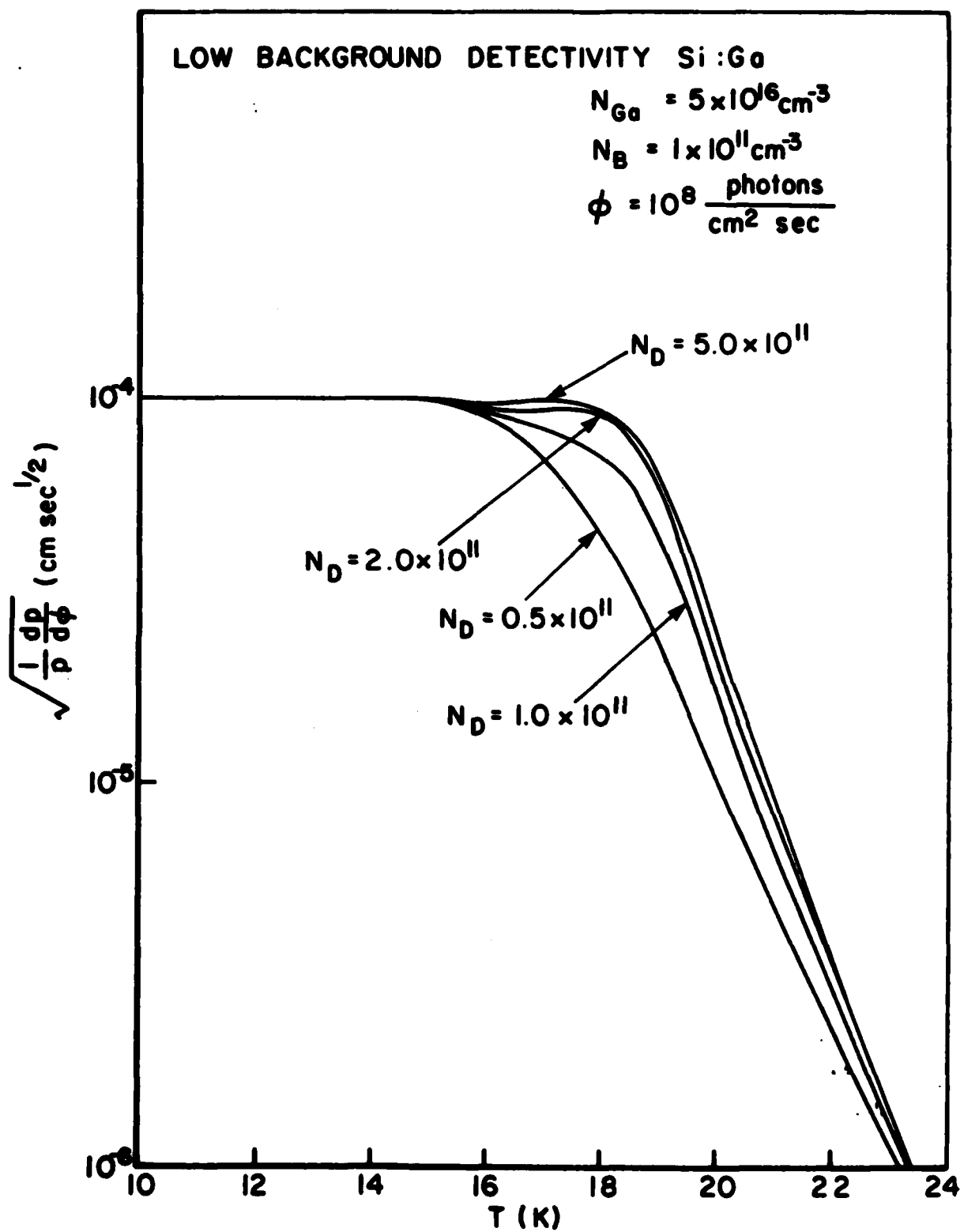


Figure 9. Plot of $(dp/pd\phi)^{1/2}$ versus temperature for the three cases (a), (b), and (c) shown in Figure 5.

Figure 10 compares the detectivities for the three cases $N_B = N_D = 10^{11}$, $N_B = N_D = 10^{13}$, and $N_B = 10^{11}$ with $N_D/N_B = 5.0$. For equal compensation there is a 25% advantage for the low boron material in the detectivities at approximately 15.5K at the same time there is also a 2.5K advantage gained in the operating temperature of the detector. Overcompensation of the boron level increases the operating temperature of the detector still further by approximately another 2.5K. However, such an increase is only obtained at the expense of reduced responsivity.

With reference to Figure 7 the overcompensation of low boron material still results in higher responsivities than for equal compensation in high boron material. Furthermore, the uniformity of response will be better for the former than for the latter case. Since in the former one is on a gently sloping portion of the $dp/d\phi$ vs. N_D/N_B curve and the latter on a highly peaked portion, small nonuniformities in the compensation ratio result in large differences in responsivity across a detector. In Figure 11 one can see that for a $\pm 10\%$ variation in the compensation ratios, $K = N_D/N_B$, the responsivity varies by as much as $\pm 60\%$ around $K=1$ for the high boron concentration material. The corresponding variation for the low boron case is only about $\pm 15\%$. In overcompensated samples, $K \gg 1$, one expects approximately $\pm 15\%$ variation in responsivity for $\pm 10\%$ variation in K .

The uniformity of response is the most critical parameter in high density detector arrays. With present-day materials, the manufacturer is often forced to trade high response for increased uniformity by greatly overcompensating the materials. By using a purer starting material, however, dramatic improvements in uniformity are consistent with high responsivity as shown graphically in Figure 11.

We also note that lower boron samples will require less neutron transmutation doping in order to achieve optimum compensation. The benefits accrued from reduced processing consist of less lattice damage, which also leads to higher carrier lifetimes and mobilities.

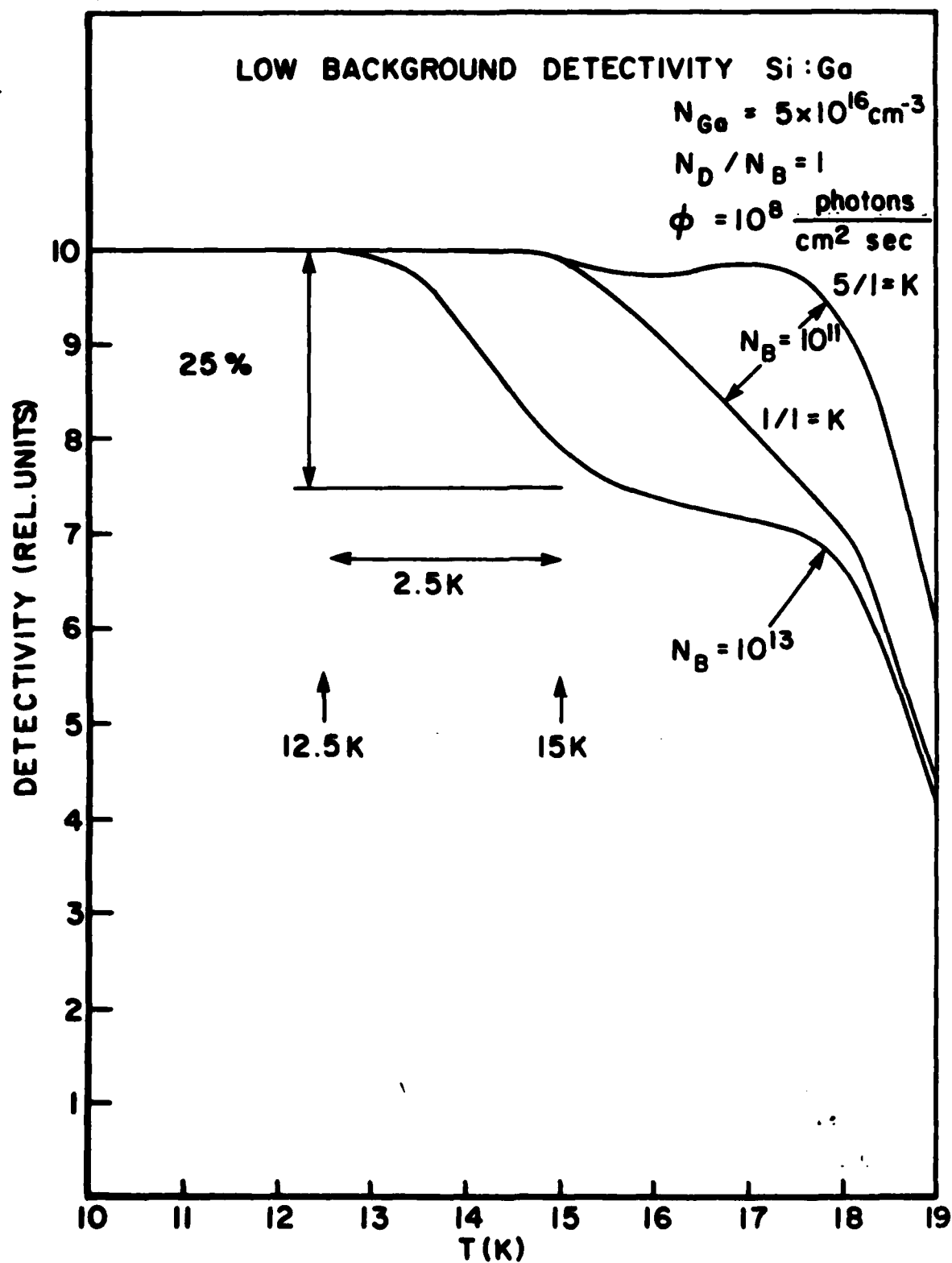


Figure 10. Comparison of $(dp/pd\phi)^{1/2}$ versus temperature for the three cases $N_D = N_B = 10^{12} \text{ cm}^{-3}$, $N_D = N_B = 10^{11} \text{ cm}^{-3}$ and $N_D = 5N_B$ ($N_B = 1 \times 10^{11} \text{ cm}^{-3}$).

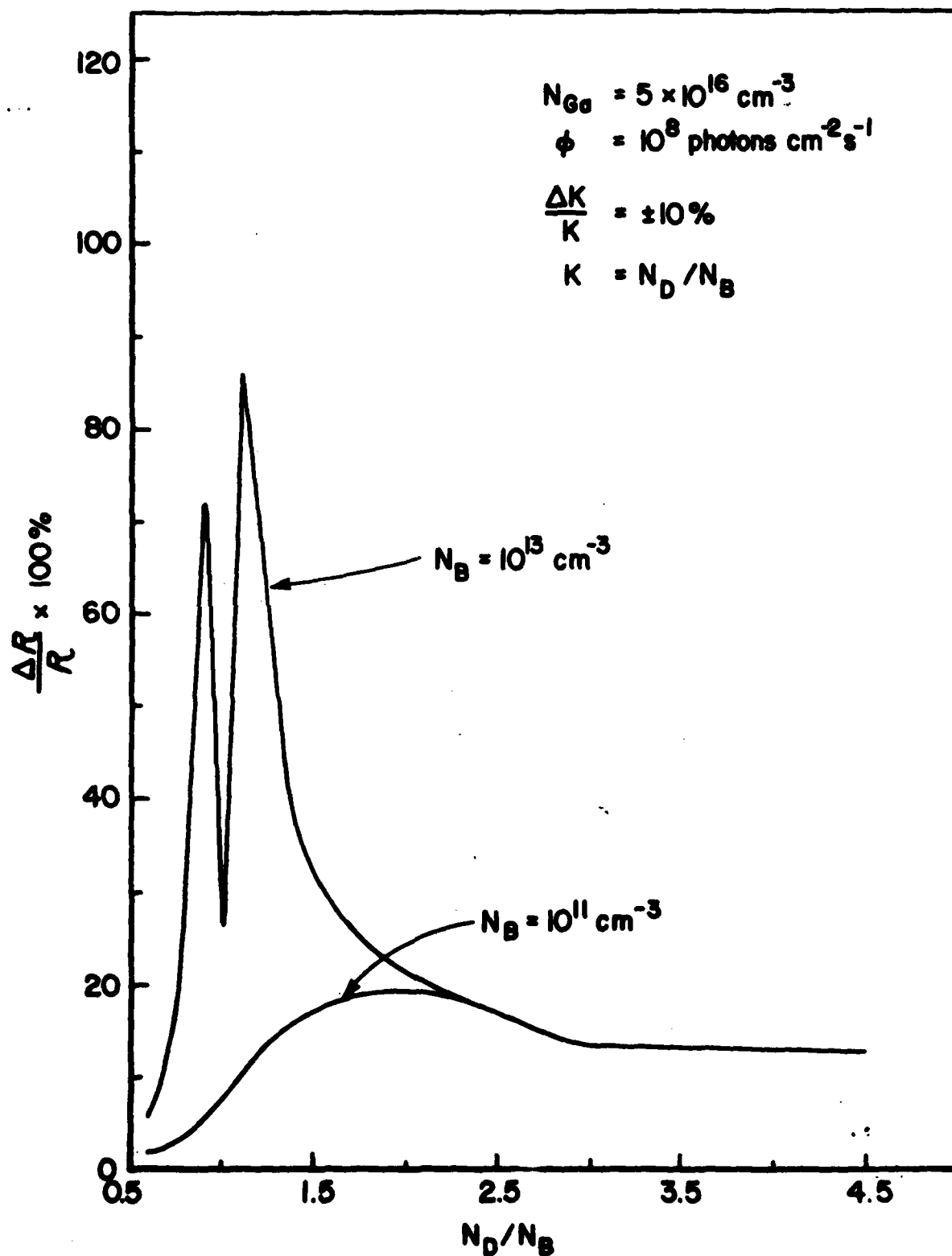


Figure 11. Plot of percentage relative error in responsivity versus compensation ratio, K , for an assumed 10% error in compensation for $N_B = 10^{11} \text{ cm}^{-3}$ and $N_B = 10^{13} \text{ cm}^{-3}$.

Fewer compensated centers, i.e. reduced concentrations of ionized boron and phosphorus, make the device more radiation hard due to the reduction in the so-called Kolbesen effect. When a high energy ionizing radiation passes through the detector it produces electron-hole pairs. The electron can fall into the empty donor level and the hole into an empty acceptor level. These levels are now free to respond to the incident signal radiation. Given the fact that boron and phosphorus respond at a different wavelength than gallium the resulting response is unwanted and constitutes a spurious signal proportional to the ionizing radiation. With less boron and phosphorus these effects are minimized.

SECTION V

CONCLUSIONS

We have modelled the behavior of extrinsic p-type Si:Ga photodetectors for low background applications. Based on the results of our calculations presented in Section IV, we conclude the following.

Large improvements in the long wavelength, low background performance of IR detectors would be realized if material with a reduced concentration of shallow impurities was used in their manufacture. The radiation hardness, responsivity, and the temperature dependence of D^* are all superior in the purer material. Though not shown explicitly in this analysis, the total system D^* (i.e. signal to noise ratio), which includes the electronics that handle the detector signals, is expected to be dramatically improved because the detectors will produce more signal and the electronic noise should be constant. The purer starting material gives a great deal more "elbow-room" in device design and processing as shown by several figures. For example, it is seen in Figure 7 that as more compensation is added to improve uniformity, the resultant responsivity is flatter as a function of compensation and also much higher. Therefore, more sensitive focal planes will be available that are also far more uniform in response across the array.

The optimal compensation ratio for maximum responsivity for $N_B = 10^{13}$ and 10^{12} cm^{-3} material is $N_D/N_B = 1$. In this regard these detectors behave similarly to Si:In detectors with $N_B = 10^{13} - 10^{14} \text{ cm}^{-3}$ in high background situations.⁹ The very low boron material, $N_B = 10^{11} \text{ cm}^{-3}$, proves an exception to this rule with increasing responsivity for undercompensation, but with deleterious effects on detectivity. For all three boron concentrations at equal compensation the responsivity is a strong function of temperature and peak responsivity is achieved only over a very limited temperature range, i.e. 19-20K. Also for the case of $N_B = 10^{13}$ and 10^{12} cm^{-3} the peak responsivity is a strong function of compensation ratio. The peak responsivity increases by a factor of four

in going from $N_B=10^{13}$ to $N_B=10^{12}\text{cm}^{-3}$ material and by another factor of four in going from $N_B=10^{12}$ to $N_B=10^{11}\text{cm}^{-3}$ material at equal compensation. In addition, a reduction in the boron concentration is accompanied by a proportional increase in carrier mobility, so that the actual gain in responsivities could be as high as 1600 in going from $N_B=10^{13}$ to $N_B=10^{11}\text{cm}^{-3}$ material. From a processing point of view a low boron concentration is also desirable since the material will require less transmutation doping by neutron irradiation, thus producing less damage, longer lifetimes, and higher mobilities.

Our results for detectivity variation with temperature indicate that overcompensation of boron with phosphorus should be done in the ratio of $N_D/N_B \approx 2$. This ratio achieves the desired increase in operating temperature of the detector with the least possible concentration of phosphorus. We predict that these detectors will have an operating temperature as high as 18K. Overcompensation by an amount of phosphorus greater than 2X does not improve the BLIP temperature or the value of detectivity while it leads to a reduction in responsivity, but it may still be necessary in specific cases to reduce effects from spatial nonuniformities in the residual impurities.

If one were to seek maximum responsivity, which occurs for N_D/N_B near unity, there is a distinct advantage in using the lowest possible boron content. The detectivity of the $N_B=10^{11}\text{cm}^{-3}$ detector is 25% larger than that of the $N_B=10^{13}\text{cm}^{-3}$ detector and with a 2.5K higher operating temperature.

This analysis, it should be noted, gives the "localized" response of a material. That is to say, in a complete detector structure contact effects and space charge can be important factors which in low backgrounds may in some cases dominate device behavior. These parameters will be considered in future modeling analyses. Initial results, however, indicate that a purer, which means a lower concentration of shallow impurities, material will contribute to reduced space charge and other irregular effects observed in device structures.

REFERENCES

1. Jones, R. C., "Phenomenological description of the response and detecting ability of radiation detectors," Proc. Inst. Radio Engrs. 47, 1495 (1959).
2. Rose, A., "Concepts in photoconductivity and allied problems," p. 97, Interscience (1963).
3. Blouke, M. M., Burgett, C. B., and Williams, R. L., "Sensitivity limits for extrinsic and intrinsic infrared detectors," Infrared Phys. 13, 61 (1973).
4. McCarthy, S. E. and Autio, C. W., "Infrared detector performance in the shuttle infrared telescope facility (SIRTF)," Proc., SPIE 132, 81 (1978).
5. Sclar, N., "Development status of silicon extrinsic IR detectors, II," Proc. SPIE (1983) (to be published).
6. Blakemore, J. S., Semiconductor Statistics, Volume 3 of International Series of Monographs on Semiconductors, Ed. H. H. Hensch, Pergamon Press, NY (1962).
7. Madarasz, F. L., Lang, J. E., and Hemenger, P. M., "Effective masses for nonparabolic bands in p-type silicon," J. Appl. Phys. 52, 7, 4616 (1981); "Temperature dependent density of states effective mass in nonparabolic p-type silicon," J. Appl. Phys. 54, 6, 3612 (1983).
8. Arst, M. C., "Exploratory development on silicon material for LADIR," AFML-TR-76-125 (1978).
9. Alexander, D. H., Baron, R., and Stafsudd, O. M., "Temperature dependence of responsivity in closely compensated Si:In detectors," Proc. IRIS Detector, p. 455 (1981).

END

FILMED

9-84

DTIC